# *Using ArcMap to Extract Shorelines from Landsat TM & ETM+ Data*

*Thirty-second ESRI International Users Conference Proceedings, San Diego, CA*

Richard C. Daniels, GISP


## *Abstract*

Many site and region specific shoreline change monitoring programs use labor and time intensive methodologies for data collect. The collection, compilation, and analysis of this data can take years. This study demonstrates a low cost methodology for quantifying regional shoreline change using Landsat TM and ETM+ data. The near-continues 29 year record of TM and ETM+ data makes this a rich dataset for both decadal and annual change analysis. Using Landsat data this study derived ocean shorelines for the years 1989, 1995, 1999, 2010, 2011, 2012 for Southwest Washington and Northwest Oregon. A shoreline change trend analysis was then conducted at 1 km intervals along a 102 km long section of coast. The change rates for the period 1995 to 1999 were compared to published rates obtained from orthophotography and an R-squared of 0.79 obtained.


## INTRODUCTION

A majority of the shoreline change monitoring programs conducted by State and Local governments use historical maps or charts, air photography, and other high resolution data sets such as LiDAR and ground topographic survey to derive the shorelines used in their change analysis (e.g., Gelfenbaum and Kaminsky 2000; Gibbs et. al. 2011). These methods for deriving shoreline position are labor and time intensive, with the time between data collection and analysis often being months to years.

The use of these traditional methods is justified when detailed site specific information is required and shoreline change is being monitored at the sub-meter level. However, on sandy beaches in regions such as the U.S. Pacific Northwest the normal spring-summer variability in shoreline position is between 23 and 28 meters (Daniels et. al. 2000). In those environments the collection of shorelines with high horizontal accuracies may not be required. Instead, course low or no cost remote sensing data sources may be substituted and used to derive shorelines.

Landsat TM and ETM+ data for the United States is currently available for download from the U.S. Geological Survey's Earth Resources Observation and Science Center (EROS). Over 29 years of Landsat TM and ETM+ data are available at no or low cost from EROS. A majority of this data is terrain corrected to the L1T level. This processing level has been shown to have a nominal horizontal accuracy of +/- 1 pixel, or 30 meters (Welch and Usery 1984). Previous studies have shown that shorelines can be extracted from Landsat TM and ETM+ data (e.g., Phillips-Born et.al. 2005; Scott et. al. 2003) and that automated techniques for the quantification of beach change can successfully utilized these shorelines (Dewidar and Frihy 2010).

## METHODS

In this study shorelines for Southwest Washington and Northwest Oregon for the years 1989, 1995, 1999, 2010, 2011, and 2012 were derived from the six Landsat 5 TM and Landsat 7 ETM+ scenes listed in Table 1. A shoreline change trend analysis was then conducted at 1 km intervals along 102 km section of coast to identify areas of significant change. To validate the results of this study the change rates calculated here for the period for 1995 to 1999 were compared to rates calculated using shorelines previously digitized for the same period from 1:12,000 and 1:24,000 scale orthophotography.

**Table 1. Landsat TM and ETM+ scenes used for this study. The date and time for each scene are shown along with the actual tide elevation (ft) at the time of over-flight. Tide elevations from the NOAA Toke Point tide gage.**

| Sensor | Scene Path/Row | Date | Approximate Over flight Time | Tide Level at Toke Point, WA | Last High Tide Time | Last High Tide | Lower Low Tide Time | Lower Low Tide | Tide Stage |
|---|---|---|---|---|---|---|---|---|---|
| ETM+ | 047, 028 | 12-May-2012 | 9:44 | 1.41 | 5:24 | 6.85 | 12:06 | -0.65 | ebbing |
| TM | 047, 028 | 25-Oct-2011 | 9:34 | 7.43 | 11:06 | 9.06 | 5:06 | 0.17 | flooding |
| ETM+ | 047, 028 | 7-May-2010 | 9:44 | 4.16 | 7:18 | 5.48 | 13:48 | 0.81 | ebbing |
| TM | 047, 028 | 15-Apr-1999 | 9:34 | 4.04 | 12:36 | 7.93 | 6:18 | -1.27 | flooding |
| TM | 047, 028 | 22-May-1995 | 9:34 | 4.97 | 7:12 | 6.8 | 13:30 | 0.79 | ebbing |
| TM | 047, 028 | 10-Sep-1989 | 9:34 | 5.9 | 9:30 | 5.91 | 14:18 | 4.23 | High Tide ebbing |

## LAND COVER CLASSIFICATION

The 7-band Landsat TM and ETM+ imagery used in this study were downloaded from U.S. Geological Survey's EROS data center. In combination, the Landsat 4, 5, and 7 satellites provided 24 to 48 passes per year for all areas in the continental United States (Bryant et. al. 2002). The large number of scenes means that if difficulties are encountered in classifying an image, it may be advisable to abandon the effort and obtain an image from a different date rather than spend weeks attempting to correct a technical issue with the data.

Several Landsat band combinations were tested to determine the optimum selection of bands and transforms to use in this study. All bands were sampled to 30 m pixels, except Landsat 5 and Landsat 7 Band 6 which were resample from 120 or 60 m, respectively, to 30 m. Band combinations considered for this study are shown in Table 2. Each band combination was tested using the same Landsat 5 TM image obtained on April 15, 1999 (scene 047, 028) for Southwest Washington and Northwest Oregon. The results of each classification and band combination were then compared to a shoreline digitized from 1:24,000 scale orthorectified air photography taken on May 26, 1999. The digitized shoreline had a nominal horizontal accuracy from all error sources of +/- 11.5 m (Daniels 2001).

**Table 2. Band combinations tested for suitability for extracting ocean shorelines.**

| Band Combination | Combination | Suitable for Shoreline Extraction? |
|---|---|---|
| a. Band Slicing - NDVI | NDVI | No, breaking waves |
| b. Band Slicing – Band 5 | Band 5 (Infrared) | No, breaking waves |
| c. 4-Band Method | Band 1-3, Band 6 (resampled) | No, Time Intensive, waves |
| d. 3-Band and NDVI | Band 1-3, NDVI | No, breaking waves |
| e. Tasseled Cap | Brightness, Greenness, Wetness, uses bands 1-7 | Yes, difficult to differentiate clouds |
| f. Tasseled Cap, NDVI | Brightness, Greenness, Wetness, NDVI | Yes |

Previous studies have suggested that the calculation of a single transform, the Normalized Difference Vegetation Index (NDVI), or the use of the Infrared Band (NIR), may be suitable for water delineation and the values of the band "sliced" to identify water, bare soil, and vegetated lands. However, a majority of these studies dealt with calm water environments -lakes, bogs, or rivers. In this study it was determined that the chaotic nature of the wave environment in the near shore surf zone resulted in a high variability in the reflectance values in the red and IR bands. As a result, the NDVI ratio (Figure 2.a) and the IR band (Figure 2.b) alone were unable to adequately separate beach from the surf zone.

The use of the 4-Band method (Figure 2.c) used traditional maximum likelihood classification methods that required training signature collection to obtain land cover classifications for each scene. The land cover classes derived were merged until only two classes remained, land and sea. This method required extensive prior knowledge of the geography of the study area. In addition, the variability in the reflectance values between study years required that the training signatures be recollected and verified with a higher accuracy data source (e.g., air photography). This method did not allow for the development of a repeatable and objective method for extracting a shoreline and was abandoned due to its time intensive nature.

The 3-Band and NDVI method (Figure 2.d) used ESRI's unsupervised ISO classification algorithm to derive ten land use classes and these classes merged to obtain a binary classification (i.e., land and sea). The advantage of this method was that no training samples were required. The merging of the classes into two groups, land and sea, was done based on visual inspection and on the dendrogram created by the ISO classification process. An example of such a plot is shown in Figure 1.

**Figure 1. Example of using the dendrogram (a plot of the hierarchical relationship of the classes) to view the distance between pairs of classes and class merge sequence.**

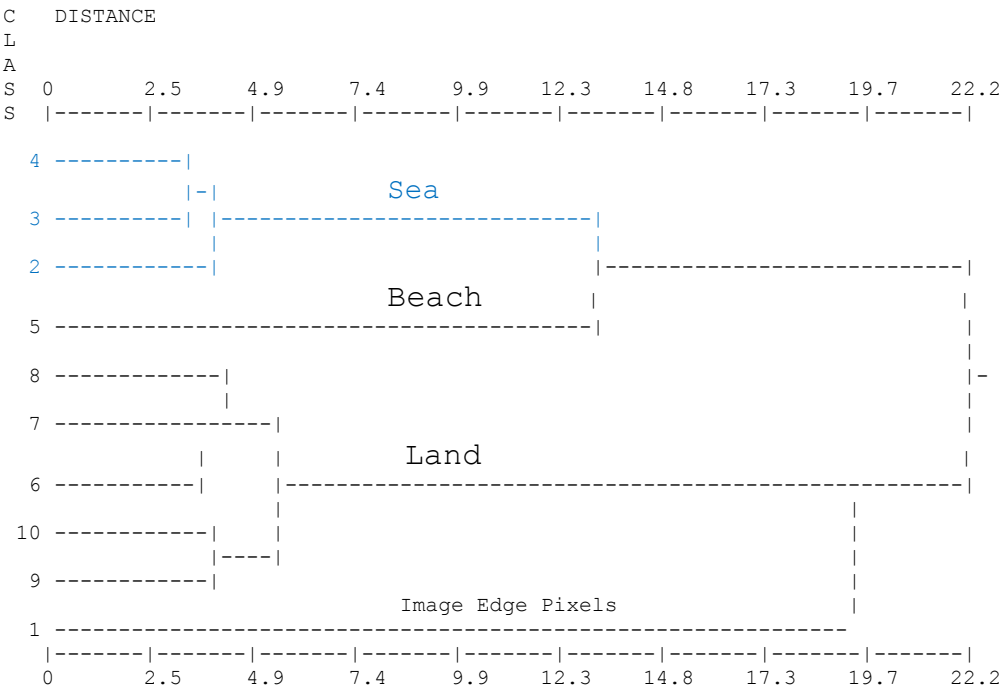


This method was fairly successful, but suffered from some of the same limitations of the 4-Band method, namely the high variability in the reflectance values in bands 1-3 made it difficult to differentiate beach from surf zone under high wave conditions.

The Normalized Difference Vegetation Index used above is only one of a set of data transformations that are available. Others include the Enhanced Vegetation Index, the Normalized Burn Ratio, and the Tasseled Cap. The Tasseled Cap has been shown to be a suitable candidate for shoreline extraction (Scott et. al. 2003).

A Tasseled-Cap Transformation converts the original bands of an image into a new set of bands with defined interpretations that are useful for vegetation mapping. The transform is calculated by taking the original image bands and created a new set of output bands based on the sum of image band 1 times a constant plus image band 2 times a constant, etc. The coefficients used in this study are for at-satellite reflectance and are from Crist, E.P. and R.C. Cicone (1984) for Landsat 5 TM data and Chenquan, H., Wylie, B., Tang, L., Homer, C. and G. Zylstra (2002) for Landsat 7 ETM+ data. Bands 1-5 and band 7 were used in the Tasseled-Cap transformation. The transformation output a set of new bands that have specific interpretations, with the number of bands output being the same as the number entered. In general, the majority of the information is contained in the first three Tasseled Cap bands which are interpreted as brightness, greenness, and wetness.

The derived brightness, greenness, wetness Tasseled Cap bands (Figure 2.e) were used as input into ESRI's unsupervised ISO classification algorithm to derive ten land use classes and these classes merged to obtain a binary classification (i.e., land and sea). The Tasseled cap did a good

job of differentiating between waves and beach, especially when the classifier option to leave 0.5% of the pixels unclassified (shown as no-data in the output) was chosen. However, in imagery with stratus clouds (high thin clouds) the differentiation between land and sea was often lost resulting in wet soil and beach being grouped into the same category as clouds.

To overcome this issue the NDVI band was added to the band combination (Figure 2.f). Charts similar to the ones shown in Figure 3 were then constructed for each year of analysis. Figure 3 compares the reflectance values found at 64 training sites of known land cover for two Landsat 5 TM scenes taken in different years –in this case 1999 and 2011. This was done to confirm that the selected transformations were able to discriminate the primary land cover types of interest in a repeatable fashion. The Tasseled Cap and NDVI combination was found to be suitable for obtaining a consistent classification from all scenes over all years for the land cover types of interest.

In general, it was found that in scenes with minimal cloud cover and low wave energies that the standard ESRI ISO unsupervised classifier could be used. In scenes with high wave energies better results were obtained by setting the rejection fraction of the classifier to 0.005. This setting allows up to 0.5% of the pixels in the image to remain unclassified. In both cases, the methodology for converting the 10 class land cover data set to land and sea was strait forward and readily automated.

**Figure 2. Comparison of the classification results obtained by each method described in Table 2 for Point Disappointment, Washington on April 15, 1999. This area is located at the mouth of the Columbia River. The shoreline shown was derived from a high accuracy orthophotography taken on May 26, 1999.**

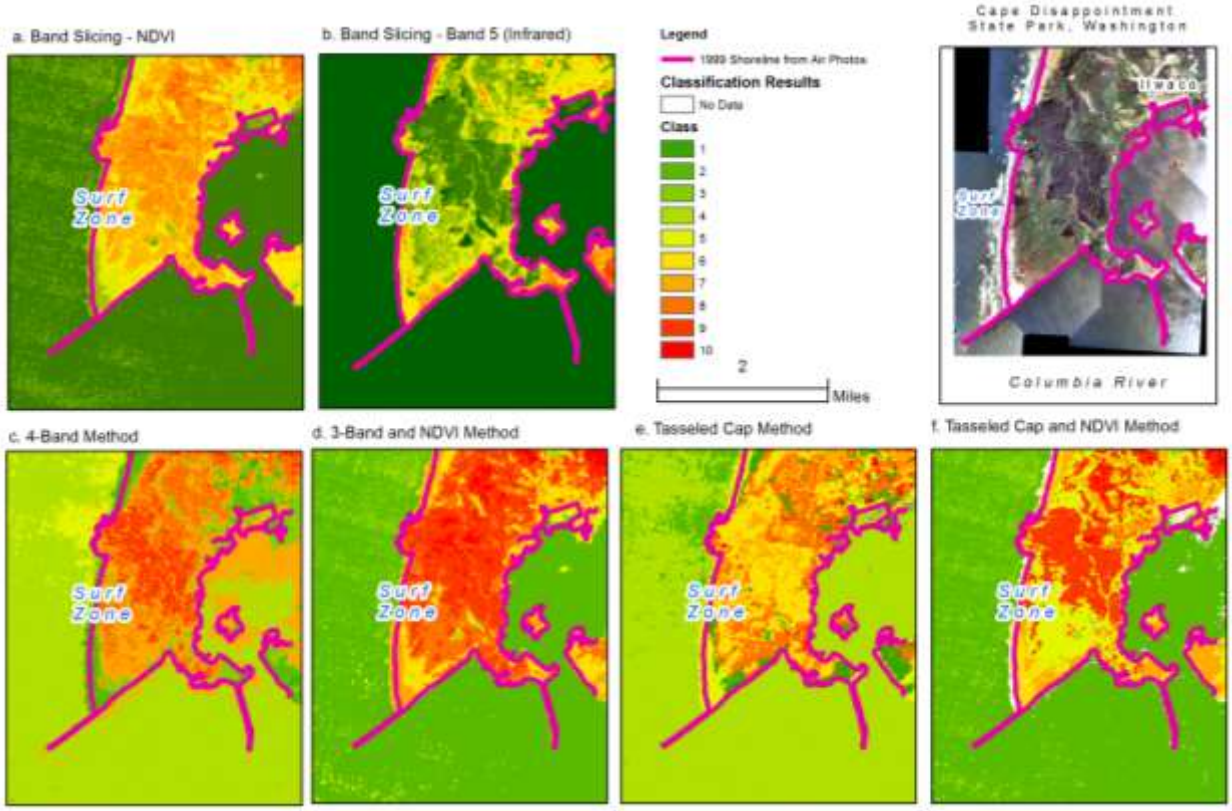


**Figure 3. Comparison of the Tasseled Cap and NDVI derived reflectance values for two Landsat 5 TM scenes taken in different years at 64 sites with known land cover.**

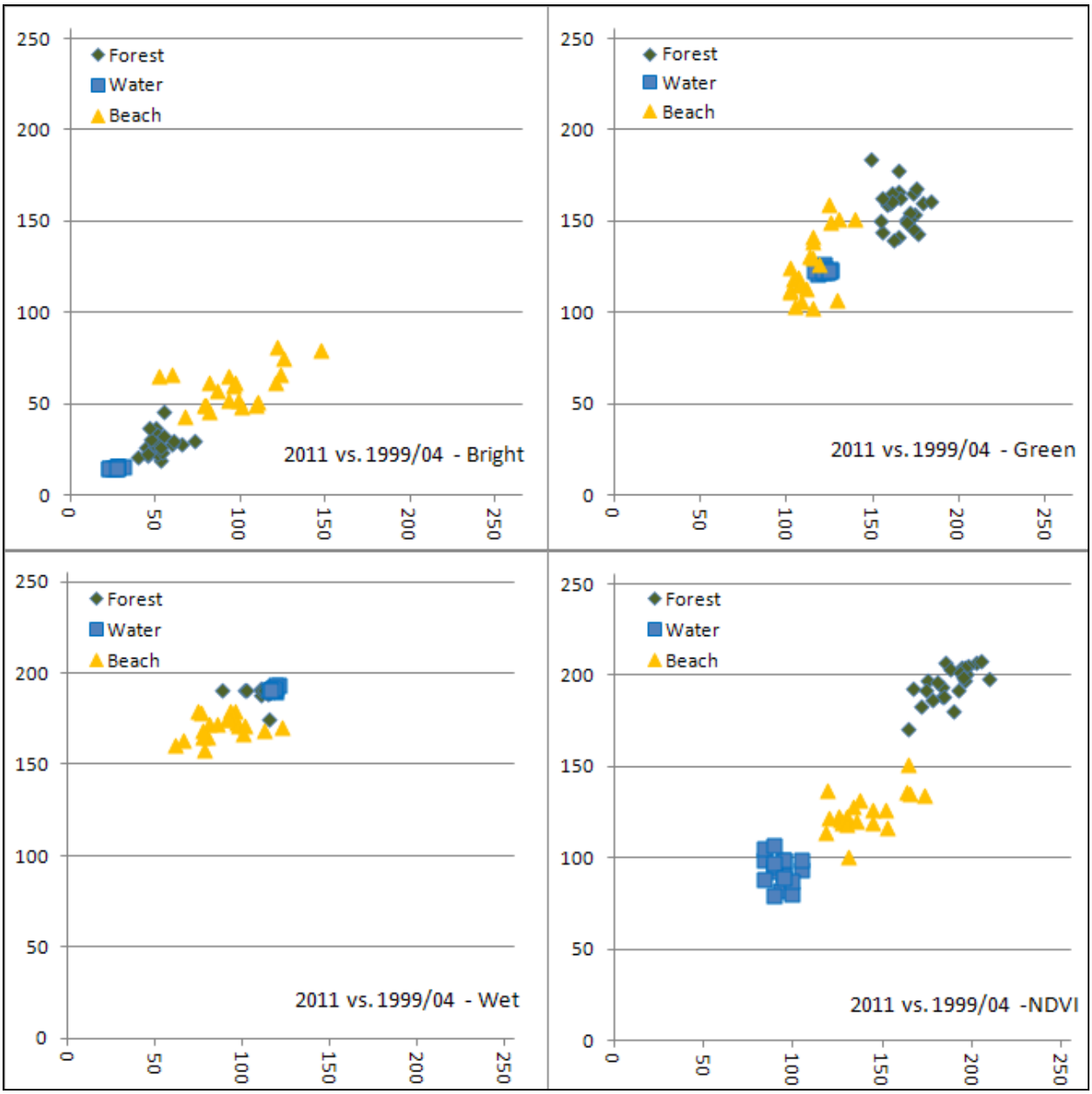


## SHORELINE CREATION

The Tasseled Cap and NDVI transformation combination was selected as the preferred combination for this study due to its ability to both normalize the data and discriminate between the surf and beach zones. To simplify the creation of shorelines from the Landsat data several models were created using ESRI's Model Builder and a custom Landsat Toolbox developed. These models, described in Table 3, helped automate and simplify many of the repetitive tasks performed when working with the Landsat TM and ETM+ datasets.

**Table 3. Listing of process steps used to obtain, classify, and processing the Landsat TM and ETM+ data for each year of interest.**

| Process Step | Process Name | Description |
|---|---|---|
| 0 | Download and Extract Data | Download data from USGS EROS Data Center and unzip. |
| 1 | Clip Multiple Rasters to AOI | Clip the imagery to the area of interest |
| 2 | Fill Landsat 7 ETM+ Scanline Errors | Fills missing data in Landsat 7 ETM+ data using the Nibble command |
| 3 | Landsat TM/ETM+ Tasseled Cap | Calculate the Tasseled Cap brightness, greenness, and wetness transformations. Normalize the bands values to 0-255. |
| 4 | NDVI | Calculate the NDVI transformation. Normalize the band values to 0-255. |
| 5 | Category Creation for Land and Sea | Take Tasseled Cap and NDVI bands as input and create a 10-class land cover data set and dendrogram. |
| 6 | Classify Land and Sea | Reclass the land cover data set from 10 to 2 classes |
| 7 | Create Shore Boundary | Create a shoreline from the 2-class land cover data set using Majority filtering, Contour, and Smooth line commands. |
| 8 | Manual Shoreline Review | Correct for cloud/surf/beach overlap |

Using the eight step processing sequence listed in Table 3 it is possible to download the raw data, classify, and extract a shoreline from a scene in 2 hours. This rapid turnaround makes it possible to create a shoreline 'on demand' and in some cases in near real-time. For example, the 2012 shoreline calculated by this study was created from imagery downloaded from EROS on May 25$^{th}$ and collected on May 12, 2012. Diagrams showing the models used in this study are contained in the Appendix A.

## SHORELINE ACURACY ASSESSMENT

One of the goals of this study was to demonstrate that accurate shorelines could be extracted from Landsat TM and ETM+ data and that shoreline change rates made using them are comparable to change rates derived from air photography. To test the validity of this hypothesis, Landsat shorelines derived for 1995 and 1999 were compared to shorelines previously digitized from 1:12,000 and 1:24,000 scale orthorectified air mosaics and the calculated change rates compared.

Rates were calculated using the Digital Shoreline Analysis System (DSAS) version 4.3, an ArcGIS extension for calculating shoreline change developed by the USGS (Thieler et. al. 2009). The summary results from this analysis are shown in Table 4 for each shoreline pair. The change rates differences were calculated for 1-km transects for 102 km of ocean shoreline.

**Table 4. Shoreline distances calculated with Landsat TM derived shorelines compared to shorelines derived from orthorectified air photography for 102 transects at 1-kilometer spacing on the Southwest Washington and Northwest Oregon coast.**

| Data Set | Horizontal Accuracy (m) | Within Pair Difference (m) | Between Pair Difference (m) |
|---|---|---|---|
| Landsat 5 TM 6/22/1995 | 30 | Mean= 41.96<br>Minimum= 0.76<br>Maximum= 245.04<br>Corrected Max= 131.97 | **Landsat 1995 to 1999** |
| 1:12,000 Scale Othophotography 9/22/1995 | 28 | | Mean= 9.34<br>Minimum= -227.31<br>Maximum= 667.04 |
| Landsat 5 TM 4/15/1999 | 30 | Mean= 34.70<br>Minimum= 2.56<br>Maximum= 94.73 | **Air Photo 1995 to 1999** |
| 1:24,000 Scale Othophotography 5/26/1999 | 23 | | Mean= -0.25<br>Minimum= -250.77<br>Maximum= 610.72 |

The within pair mean of the differences for both the 1995 and 1999 pairs indicate that the Landsat derived shorelines are systematically placed 30 to 40 m seaward of shorelines derived from air photography. The minimum within pair differences over all 102 transects approaches zero in both cases, indicating that this offset is not random. Visual inspection of the shoreline differences at each transect determined that the high within pair maximum values in 1995 occurred at locations where high altitude clouds obscured the shoreline (Figure 4) or where DSAS had encountered offshore sandbars when calculating the change rates. In these cases a single manual editing pass over the derived shoreline (using the Tasseled Cap brightness band as a backdrop) corrected the issue and reduced the maximum difference value to 131.97 m.

The between pair analysis used the edited Landsat shorelines that were corrected for clouds. The summary statistics for the between pair distances are nearly identical when the horizontal accuracies of the data sources are considered. A regression analysis was performed for the between pair change rates and an R-squared of 0.79 obtained with a standard error of 11.29 meters. Figure 5 contains a scatter diagram that compares the calculated Landsat and Air Photo derived change rates for 1995 and 1999.

The within pair analysis determined that the Landsat derived shorelines tend to be systematically place 34 to 42 m seaward of the same shoreline as derived from a 1:12,000 or 1:24,000 scale air photograph. This is not unexpected, since Landsat derived shorelines reflect the instantaneous location of the transition zone between ‘wet’ and ‘dry’ at the time the image was taken while the air photo shorelines reflect a manually digitized average high water line that is visually located “just seaward of the drift line left by the last high tide” (Daniels et. al. 2000). The between pair analysis determined that change rates have a high correlation (R squared of 0.79). The high correlation indicates that when the standard error and horizontal accuracy of the data sources are considered, that Landsat derived shorelines can be used to obtain valid shoreline change rates and that these rates are comparable to those derived from air photography.

**Figure 4. Example of high altitude clouds in Landsat 5 TM imagery obscuring portions of the coast. Shoreline derived with the automated extraction techniques used in this study may be offset seaward when they pass through obscured areas.**

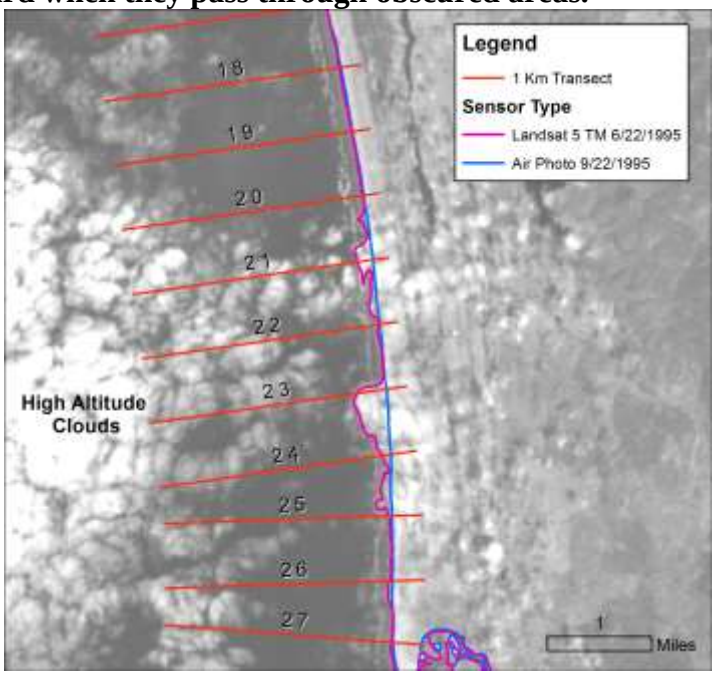


**Figure 5. Scatter diagram showing the correlation between Landsat derived shoreline change rates versus Air Photo derived rates for the period 1995 -1999. Data are for 1-km transects covering 102 km of shoreline in Southwest Washington and Northwest Oregon.**

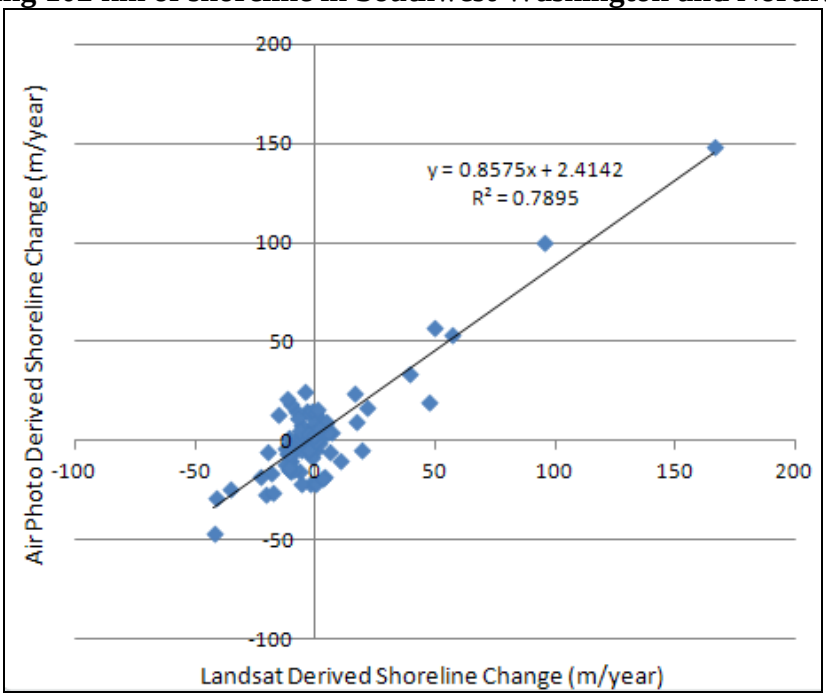


## CHANGE ANALYSIS

Rates were calculated using DSAS from shorelines for the years 1989, 1995, 1999, 2011, and 2012 (Thieler et. al. 2009). The end point rate (EPR), confidence of the EPR rate (ECI), linear regression rate (LRR), and confidence of the LRR rate at the 95% confidence interval (LCI95) were calculated for each transect using all available shorelines for the 1989-2012 period. In addition, EPR rates were calculated separately for the period 1989 to 1999 and 1999 to 2012 to see if a change in trend could be identified (Figure 6). The calculated change rates used to construct Figure 6 are listed in Appendix B.

**Figure 6. End point change rates for 102 transects in m/year for North Cove, Washington, Long Beach, Washington and Seaside, Oregon for the periods 1989 to 1999, 1999 to 2012, and 1989 to 2012. Black transects indicate erosion or accretion rates that fall within the uncertainty of the data at the 95% confidence level.**

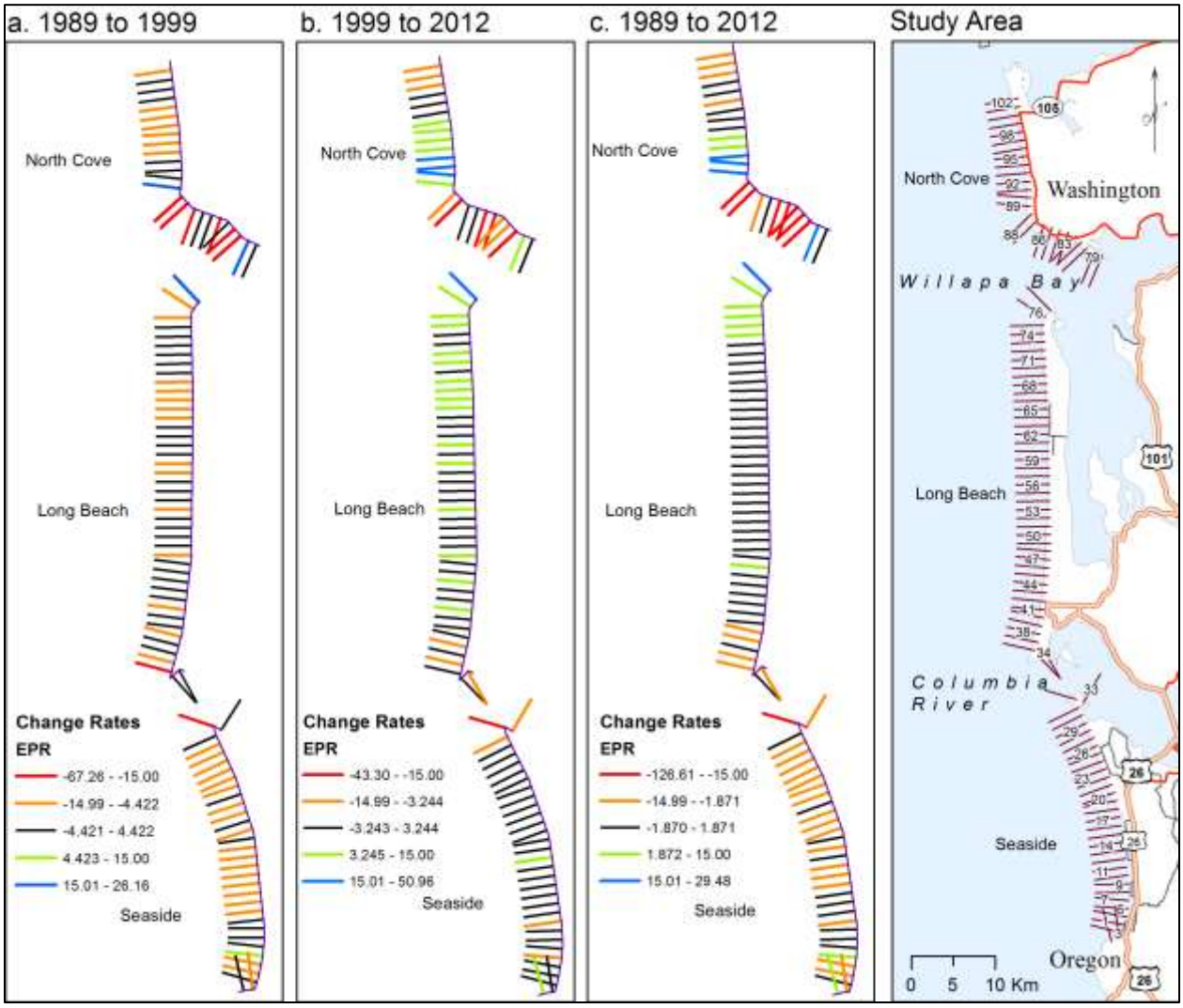


The EPR change rates shown in Figure 6 correctly identify the known high erosion rate areas in the study area (Gelfenbaum and Kaminsky 2000). Of note is the rapidly eroding area on the

south side of North Cove, WA due to the northward migration of the Willapa Bay channel near transects 80-88. A large amount of this sediment is transported northward by alongshore currents and deposited on the western shoreline of North Cove (transects 89-96). In Long Beach, WA the northern tip of the peninsula (transect 77) has grown northward during the entire period of record at about the same rate as North Cove has eroded. The southern 5-km of Long Beach adjacent to the Columbia River and the rivers North Jetty (transect 36-40) has seen long term erosion. In Seaside, OR in the 1989 to 1999 period we see a general erosion trend along a majority of the coast (except at the mouth of a river near transect 5-7). In addition, erosion was seen adjacent to the Columbia River at the South Jetty (transect 31-33). After 1999 there was a general reversal of trend to accretion. However when taken in total a majority of the Seaside area has experienced net erosion over the last 23 years.

## CONCLUSION

Using Landsat data this study derived ocean shorelines for the years 1989, 1995, 1999, 2010, 2011, 2012 for Southwest Washington and Northwest Oregon and conducted a change analysis at 1 km intervals along a 102 km section of the shoreline. Change rates calculated using the Landsat derived shorelines for the period 1995 to 1999 were compared to published rates obtained from orthorectified 1:12,000 and 1:24,000 scale air photography and an R-squared of 0.79 obtained. This high correlation indicates that change rates derived from shorelines extracted from Landsat TM and ETM+ data are comparable to rates derived from high accuracy air photography.

This study successfully demonstrated a low cost methodology for using Landsat TM and ETM+ data for quantifying regional shoreline change in high wave energy beach environments -such as found in the Pacific Northwest. The near-continues 29 year record of TM and ETM+ data makes this a rich dataset for both decadal, annual, and seasonal change analysis.

In the annual or seasonal time frames, this methodology may be used for monitoring river or inlet migration and the movement of ephemeral features such as large sandbars or rapidly migrating barrier islands. Figure 7 shows an example of how Landsat derived shorelines could be used to monitor change at a bay inlet, in this case for Willapa Bay, Washington. Table 1 shows the tide level at the time of over flight for each shoreline. For the shorter time periods shown (Figure 7.d., 7.e., and 7.f.), the calculation of change rates would require the implementation of a tide correction methodology; however, that is outside the scope of the current paper.

**Figure 7. Using Landsat derived shorelines to monitor the movement of ephemeral islands in Willapa Bay. The large sand island at the mouth of the bay in 1989 disappeared by 1999 and began to reformed further to the south by 2010**

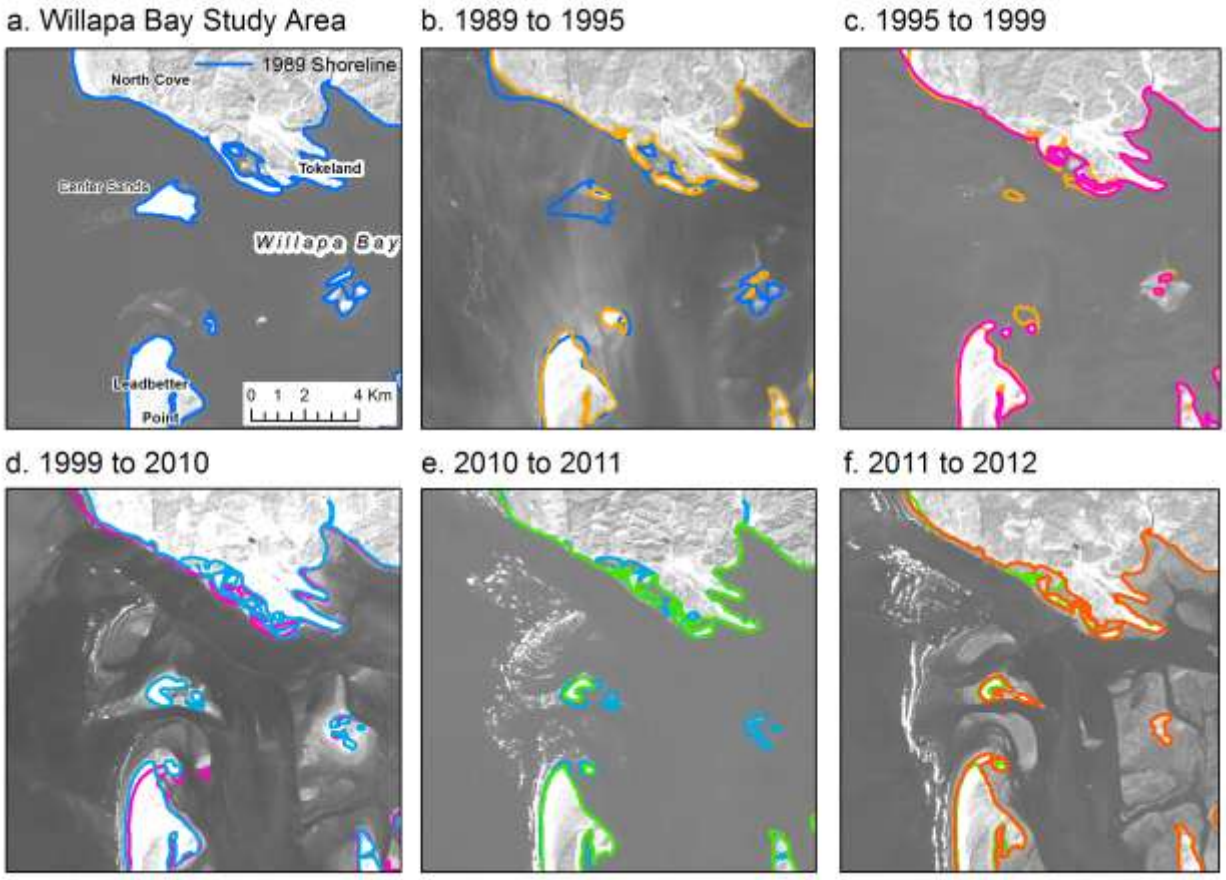


## AUTHOR INFORMATION

Richard C. Daniels, GISP
GIS Coordinator
Office of Information Technology
Washington State Department of Transportation
P.O. Box 47430
Olympia, WA 98504-7430
Phone: (360) 705-7654
FAX: (360) 705-6817
danielri@wsdot.wa.gov

## REFERENCES


Bryant, R., Moran, M.S., McElroy, S., Holifield, C., Thome, K., and T. Miura. 2002. Data continuity of Landsat-4 TM, Landsat-5 TM, Landsat-7 ETM+, and Advanced Land Imager (ALI) sensors. *IEEE International Geoscience and Remote Sensing Symposium*, 00 (C): 584-586.

Chenquan, H., Wylie, B., Tang, L., Homer, C. and G. Zylstra. 2002. Derivation of a Tasseled Cap Transformation Based on Landsat 7 At-Satellite Reflectance. *International Journal of Remote Sensing*, 23(8): 1741-1748. Available online at http://landcover.usgs.gov/pdf/tasseled.pdf.

Crist, E.P. and R.C. Cicone. 1984. A physically-based transformation of Thematic Mapper data – the TM Tasseled Cap. IEEE Transactions on Geoscience and Remote Sensing, GE-22 (3): 256-263.

Daniels, R.C. 2001. Calculating coastal change rates for Northwest Oregon and Southwest Washington. NOAA Coastal Services Center, Coastal Geotools'01, *Proceedings of the 2nd Biennial Coastal GeoTools Conference*, Charleston, SC.

Daniels, R.C., Ruggiero, P., and McCandless, D. 2000. Interpretation of the average high water line from aerial photography: Variability and repeatability. In Southwest Washington Coastal Erosion Workshop Report, 1999, U.S. Geological Survey Open-File Report 00-439, pp. 58-74. Available online at http://pubs.usgs.gov/of/2000/of00-439/.

Dewidar, K.M. and O.E. Frihy. 2010. Automated techniques for quantification of beach change rates using Landsat series along the North-eastern Nile Delta, Egypt. *Journal of Oceanography and Marine Science*, 1(2): 28-39.

Gelfenbaum, G. and G.M. Kaminsky (eds.). 2000. Southwest Washington Coastal Erosion Study Workshop Report 1999. U.S. Geological Survey Open-File Report 00-439. Available online at http://pubs.usgs.gov/of/2000/of00-439/.

Gibbs, A.E., Harden, E.L., Richmond, B.M., and L.H. Erikson. 2011. Regional shoreline change and coastal erosion hazards in Arctic Alaska. In Solutions to Coastal Disasters 2011 - Proceedings of the 2011 Solutions to Coastal Disasters Conference, American Society of Civil Engineers, Reston, VA.

Phillips-Born, K., C. Locke, J. Michel, and D. Braud. 2005. *Feasibility of using remote-sensing techniques for shoreline delineation and coastal habitat classification for environmental sensitivity index (ESI) mapping*. U.S. Dept. of the Interior, Minerals Management Service, Gulf of Mexico OCS Region, New Orleans, LA. OCS Study MMS 2005-047. Available online at http://www.data.boem.gov/PI/PDFImages/ESPIS/4/4224.pdf.

Scott, J.W., Moore, L.R., Harris, W.M., and M.D. Reed. 2003. *Using the Landsat Enhanced Thematic Mapper Tasseled Cap Transformation to Extract Shoreline*. U.S. Geological Survey, Open-File Report OF 03-272. Available online at http://pubs.usgs.gov/of/2003/0272/.

Thieler, E.R., Himmelstoss, E.A., Zichichi, J.L., and Ergul, Ayhan, 2009, Digital Shoreline Analysis System (DSAS) version 4.0—An ArcGIS extension for calculating shoreline change: U.S. Geological Survey Open-File Report 2008-1278. Available online at http://pubs.usgs.gov/of/2008/1278/.

Welch, R. and E.L. Usery. 1984. Cartographic accuracy of Landsat-4 MSS and TM image data. *IEEE Transactions on Geoscience and Remote Sensing,* GE-22 (3): 281-288.

## DISCLAIMER

## APPENDIX A

The following screen captures from ArcGIS Desktop show the schematic design of the models used in this study. These models were grouped and saved into a "Landsat Toolbox" that greatly simplified and streamlined the raster classification and shoreline extraction process. This Toolbox is available upon request to the author.

**Table A-1. Schematic diagrams showing the models created with ESRI's Model Builder tool in ArcMap for used in this study.**

Clip Multiple Rasters to AOI

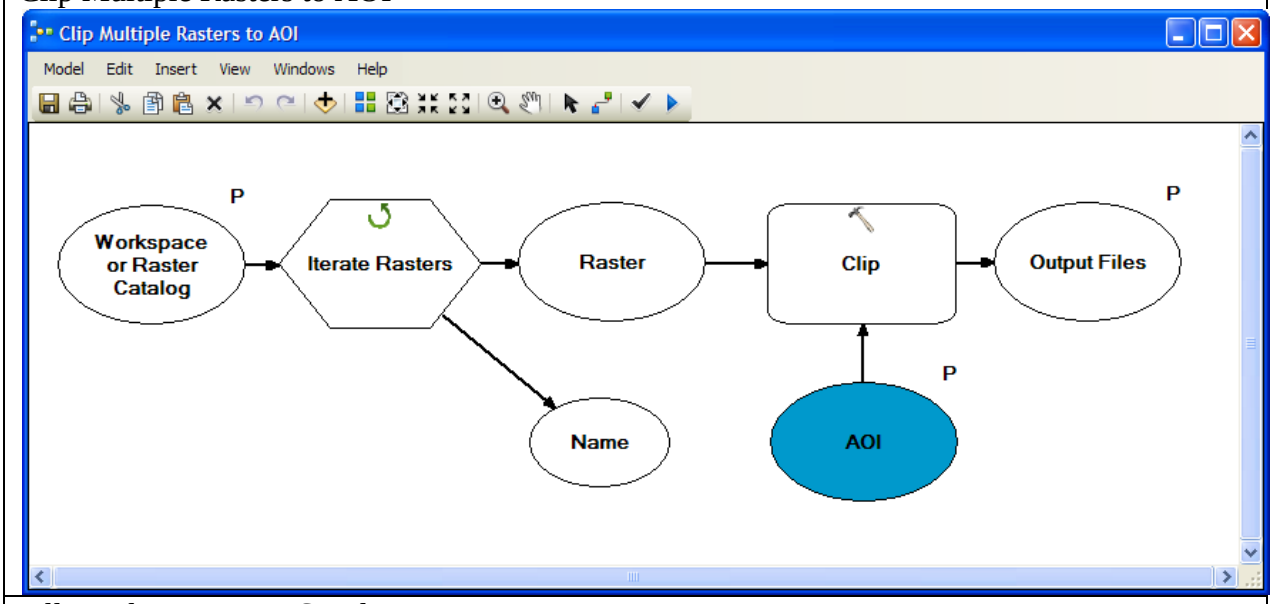


Fill Landsat 7 ETM+ Scanline Errors

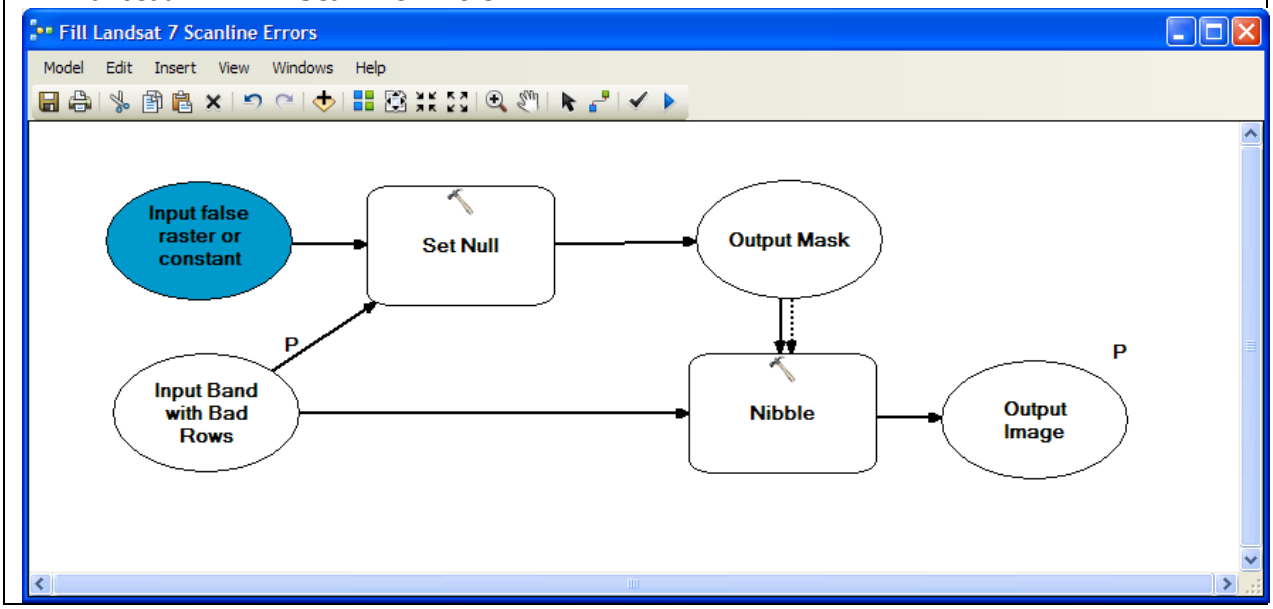

Landsat 5 TM Tasseled Cap

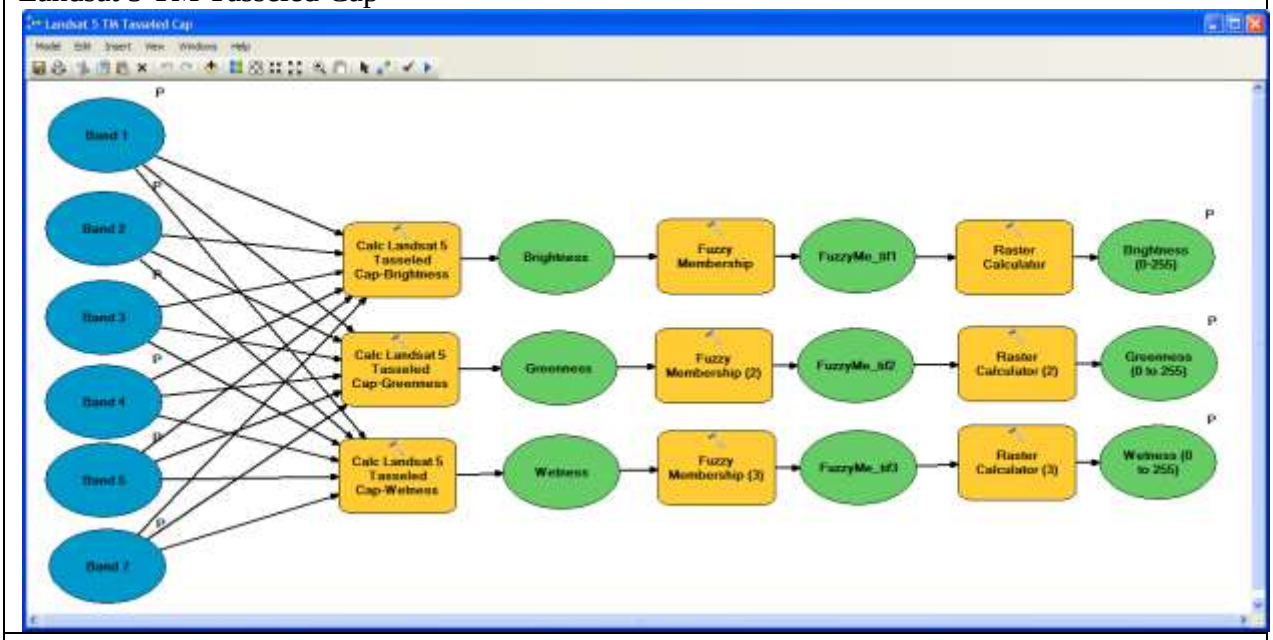


Landsat 7 ETM+ Tasseled Cap

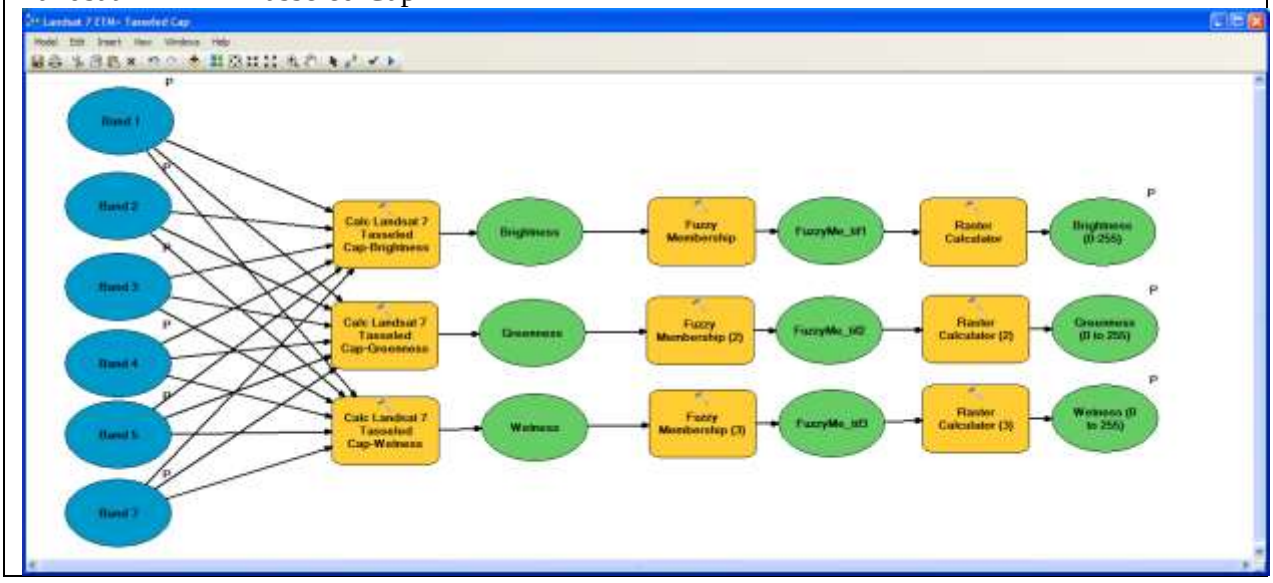

NDVI

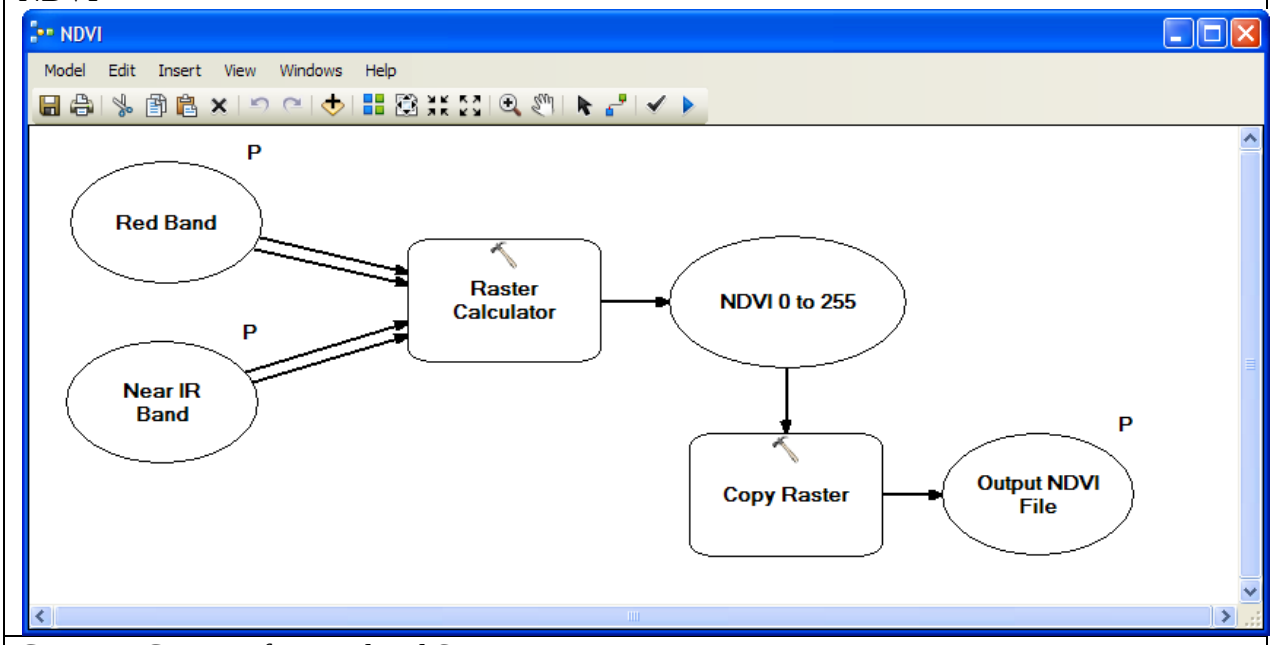


Category Creation for Land and Sea

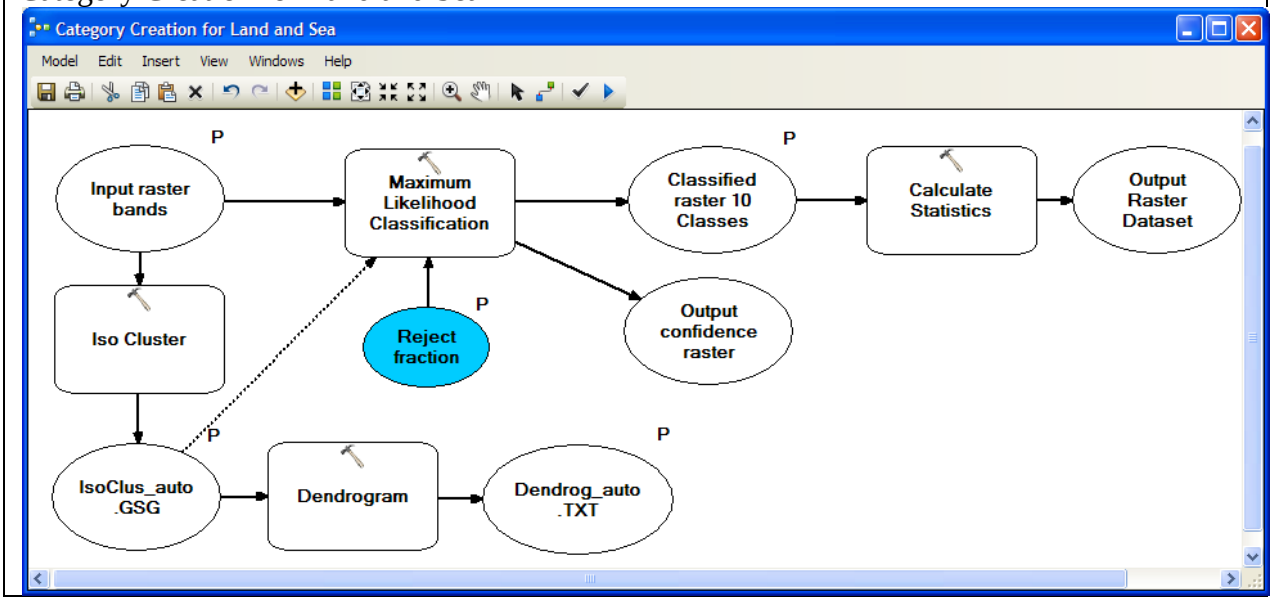

Classify Land and Sea

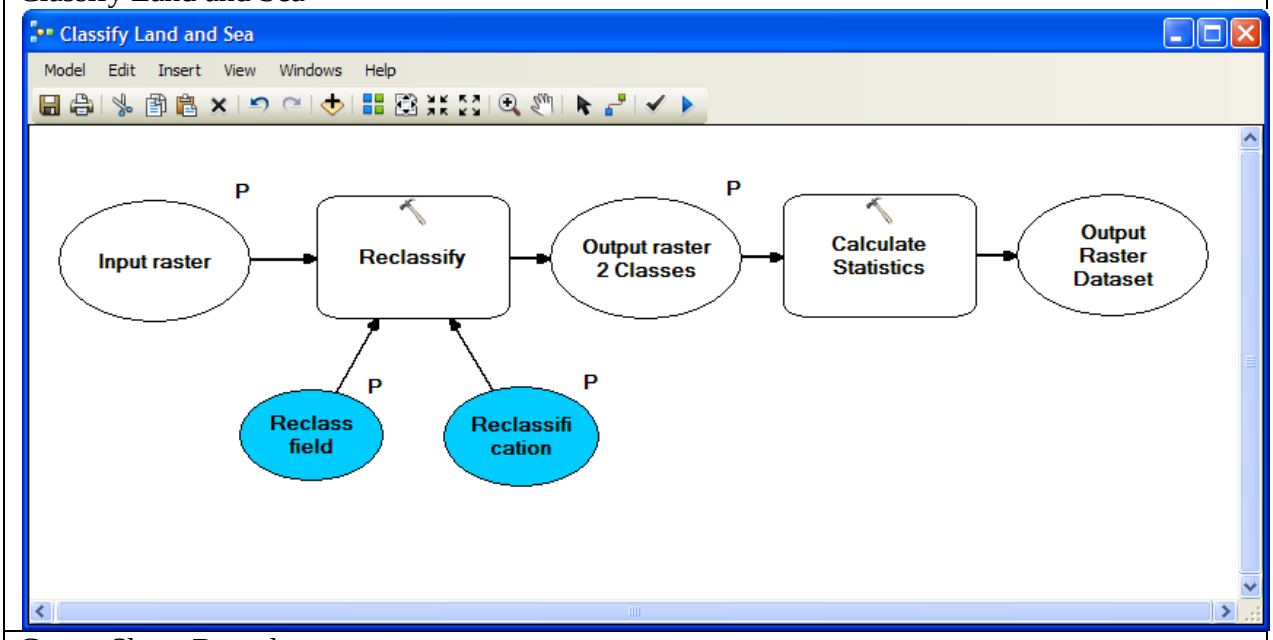


Create Shore Boundary

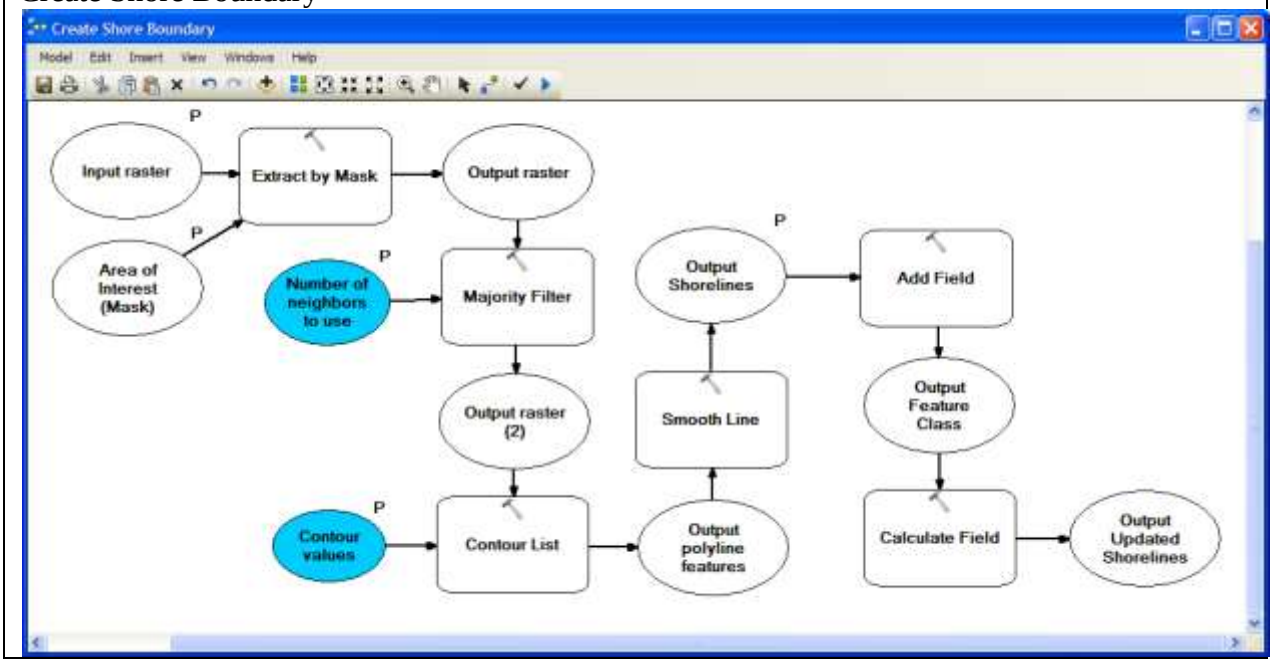

## APPENDIX B

Table B-1 shows calculated change rates for the periods 1989 to 1999, 1999 to 2012, and 1989 to 2012 as calculated by DSAS (Thieler et. al. 2009). The End Point Rates (EPR) and the End Point Confidence intervals (ECI) are shown for each period. The ECI can be though off as the 95% confidence interval and can be used as a +/- value. For example, transect 1 for the period 1989 to 2012 hand an accretion rate of 2.57 m/year +/- 1.87 m/year at the 95% confidence level.

The LRR calculation utilized all five Landsat shorelines derived for this study for the years 1989, 1995, 1999, 2011, 2012. The Linear Regression Rate (LRR) for transect 1 for the period 1989 to 2012 is 0.52 m/year with a Linear Regression Confidence Interval at the 95% level (LCI95) of +/- 7.20 m/year. The large difference between the EPR rate and LRR rate for this transect indicates a reversal of trend occurred at this location during the analysis period.

**Table B-1. Change rates for the periods 1989 to 1999, 1999 to 2012, and 1989 to 2012 for North Cove, Washington, Long Beach, Washington, and Seaside, Oregon.**

| Transect ID | StartX (m) | StartY (m) | Azimuth (Degrees) | EPR 1989 to 1999 | ECI 1989 to 1999 | EPR 1999 to 2012 | ECI 1999 to 2012 | EPR 1989 to 2012 | ECI 1989 to 2012 | LRR 1989 to 2012 | LCI95 1989 to 2012 | Region |
|---|---|---|---|---|---|---|---|---|---|---|---|---|
| 1 | 426436.08 | 5091307.88 | 345.32 | -0.60 | 4.42 | 4.89 | 3.24 | 2.57 | 1.87 | -0.47 | 6.16 | Seaside |
| 2 | 427418.95 | 5091486.31 | 351.30 | -12.34 | 4.42 | -2.79 | 3.24 | -6.83 | 1.87 | -7.37 | 3.13 | Seaside |
| 3 | 427866.82 | 5092235.88 | 284.50 | -1.67 | 4.42 | 0.75 | 3.24 | -0.27 | 1.87 | -1.28 | 1.92 | Seaside |
| 4 | 428075.01 | 5093213.42 | 280.59 | -7.14 | 4.42 | 0.65 | 3.24 | -2.65 | 1.87 | -3.01 | 4.16 | Seaside |
| 5 | 428258.82 | 5094196.38 | 280.59 | -8.90 | 4.42 | 1.25 | 3.24 | -3.05 | 1.87 | -3.35 | 3.30 | Seaside |
| 6 | 428416.57 | 5095182.77 | 274.49 | 14.83 | 4.42 | -6.15 | 3.24 | 2.73 | 1.87 | 4.87 | 12.86 | Seaside |
| 7 | 428493.39 | 5096179.81 | 274.41 | -3.15 | 4.42 | 2.37 | 3.24 | 0.03 | 1.87 | -1.50 | 3.13 | Seaside |
| 8 | 428508.40 | 5097178.25 | 268.18 | -3.31 | 4.42 | 0.14 | 3.24 | -1.32 | 1.87 | -2.11 | 2.31 | Seaside |
| 9 | 428476.60 | 5098177.75 | 268.18 | -3.44 | 4.42 | 0.22 | 3.24 | -1.33 | 1.87 | -2.10 | 2.80 | Seaside |
| 10 | 428382.05 | 5099171.76 | 261.84 | 0.20 | 4.42 | -3.41 | 3.24 | -1.88 | 1.87 | -3.39 | 3.62 | Seaside |
| 11 | 428240.08 | 5100161.63 | 261.84 | -4.78 | 4.42 | 1.21 | 3.24 | -1.33 | 1.87 | -1.54 | 2.20 | Seaside |
| 12 | 428098.11 | 5101151.50 | 261.84 | -5.37 | 4.42 | 1.60 | 3.24 | -1.35 | 1.87 | -1.02 | 2.38 | Seaside |
| 13 | 427956.14 | 5102141.37 | 261.84 | -5.02 | 4.42 | 1.55 | 3.24 | -1.23 | 1.87 | -1.77 | 2.20 | Seaside |
| 14 | 427814.17 | 5103131.24 | 261.84 | -4.80 | 4.42 | -0.28 | 3.24 | -2.19 | 1.87 | -1.90 | 2.46 | Seaside |
| 15 | 427672.20 | 5104121.11 | 261.84 | -8.83 | 4.42 | 1.65 | 3.24 | -2.78 | 1.87 | -2.16 | 3.54 | Seaside |
| 16 | 427530.23 | 5105110.98 | 261.84 | -8.23 | 4.42 | 0.82 | 3.24 | -3.01 | 1.87 | -2.02 | 3.10 | Seaside |
| 17 | 427388.26 | 5106100.86 | 261.84 | -8.33 | 4.42 | 3.74 | 3.24 | -1.37 | 1.87 | -1.18 | 3.56 | Seaside |
| 18 | 427246.29 | 5107090.73 | 261.84 | -8.61 | 4.42 | 2.76 | 3.24 | -2.05 | 1.87 | -1.66 | 3.36 | Seaside |
| 19 | 427083.17 | 5108077.11 | 259.46 | -4.07 | 4.42 | 1.22 | 3.24 | -1.02 | 1.87 | -0.75 | 2.58 | Seaside |
| 20 | 426819.61 | 5109038.32 | 250.12 | -4.44 | 4.42 | -0.02 | 3.24 | -1.89 | 1.87 | -2.23 | 1.85 | Seaside |
| 21 | 426479.53 | 5109978.71 | 250.12 | -3.33 | 4.42 | -1.14 | 3.24 | -2.07 | 1.87 | -2.48 | 1.02 | Seaside |
| 22 | 426139.46 | 5110919.11 | 250.12 | -7.57 | 4.42 | 0.75 | 3.24 | -2.77 | 1.87 | -2.31 | 2.95 | Seaside |
| 23 | 425799.38 | 5111859.51 | 250.12 | -5.17 | 4.42 | 1.44 | 3.24 | -1.36 | 1.87 | -1.51 | 2.18 | Seaside |

| Transect ID | StartX (m) | StartY (m) | Azimuth (Degrees) | EPR 1989 to 1999 | ECI 1989 to 1999 | EPR 1999 to 2012 | ECI 1999 to 2012 | EPR 1989 to 2012 | ECI 1989 to 2012 | LRR 1989 to 2012 | LCI95 1989 to 2012 | Region |
|---|---|---|---|---|---|---|---|---|---|---|---|---|
| 24 | 425459.30 | 5112799.91 | 250.12 | -2.15 | 4.42 | -2.45 | 3.24 | -2.32 | 1.87 | -2.24 | 4.12 | Seaside |
| 25 | 425119.22 | 5113740.30 | 250.12 | -6.05 | 4.42 | -1.20 | 3.24 | -3.25 | 1.87 | -2.57 | 2.91 | Seaside |
| 26 | 424762.76 | 5114673.69 | 244.78 | -11.15 | 4.42 | 3.02 | 3.24 | -2.98 | 1.87 | -2.86 | 4.86 | Seaside |
| 27 | 424317.19 | 5115568.94 | 243.54 | -12.50 | 4.42 | 2.03 | 3.24 | -4.12 | 1.87 | -3.08 | 5.62 | Seaside |
| 28 | 423871.62 | 5116464.18 | 243.54 | -8.34 | 4.42 | -1.97 | 3.24 | -4.67 | 1.87 | -2.98 | 3.81 | Seaside |
| 29 | 423426.05 | 5117359.43 | 243.66 | -9.91 | 4.42 | -2.64 | 3.24 | -5.72 | 1.87 | -4.50 | 3.15 | Seaside |
| 30 | 422984.66 | 5118256.74 | 243.82 | -8.99 | 4.42 | -1.37 | 3.24 | -4.59 | 1.87 | -3.70 | 4.04 | Seaside |
| 31 | 422543.43 | 5119154.14 | 243.82 | 1.06 | 4.42 | -3.26 | 3.24 | -1.43 | 1.87 | -2.30 | 3.44 | Seaside |
| 32 | 422302.51 | 5120111.90 | 286.32 | -20.25 | 4.42 | -23.90 | 3.24 | -22.36 | 1.87 | -21.88 | 15.78 | Seaside |
| 33 | 423057.23 | 5119751.29 | 31.09 | -3.44 | 4.42 | -11.45 | 3.24 | -8.06 | 1.87 | -8.71 | 3.08 | Seaside |
| 34 | 418253.30 | 5126174.06 | 149.31 | -4.07 | 4.42 | -6.91 | 3.24 | -5.71 | 1.87 | -3.83 | 4.17 | Long Beach |
| 35 | 417532.89 | 5125480.51 | 136.09 | -1.25 | 4.42 | -2.12 | 3.24 | -1.76 | 1.87 | -1.36 | 0.88 | Long Beach |
| 36 | 417456.62 | 5125926.94 | 282.85 | -23.63 | 4.42 | -0.28 | 3.24 | -10.16 | 1.87 | -10.55 | 7.44 | Long Beach |
| 37 | 417678.99 | 5126901.90 | 282.85 | -5.62 | 4.42 | -6.99 | 3.24 | -6.41 | 1.87 | -7.02 | 2.46 | Long Beach |
| 38 | 417901.36 | 5127876.86 | 282.85 | -0.14 | 4.42 | -0.93 | 3.24 | -0.60 | 1.87 | -1.05 | 2.29 | Long Beach |
| 39 | 418123.73 | 5128851.82 | 282.85 | -1.20 | 4.42 | -5.65 | 3.24 | -3.77 | 1.87 | -3.40 | 6.77 | Long Beach |
| 40 | 418346.11 | 5129826.78 | 282.85 | -7.60 | 4.42 | 0.66 | 3.24 | -2.84 | 1.87 | -4.16 | 4.66 | Long Beach |
| 41 | 418501.27 | 5130812.48 | 275.31 | -2.66 | 4.42 | -0.35 | 3.24 | -1.33 | 1.87 | -2.38 | 2.67 | Long Beach |
| 42 | 418593.74 | 5131808.20 | 275.31 | -4.42 | 4.42 | 0.25 | 3.24 | -1.73 | 1.87 | -1.77 | 2.07 | Long Beach |
| 43 | 418686.22 | 5132803.91 | 275.31 | -11.09 | 4.42 | 5.45 | 3.24 | -1.55 | 1.87 | -1.57 | 5.03 | Long Beach |
| 44 | 418778.70 | 5133799.63 | 275.31 | -3.21 | 4.42 | 0.88 | 3.24 | -0.85 | 1.87 | -2.30 | 3.99 | Long Beach |
| 45 | 418871.18 | 5134795.34 | 275.31 | -3.77 | 4.42 | 2.37 | 3.24 | -0.23 | 1.87 | -0.06 | 3.19 | Long Beach |
| 46 | 418963.66 | 5135791.06 | 275.31 | -3.22 | 4.42 | 4.69 | 3.24 | 1.35 | 1.87 | 0.63 | 2.87 | Long Beach |
| 47 | 419056.13 | 5136786.77 | 275.31 | 0.67 | 4.42 | 3.15 | 3.24 | 2.10 | 1.87 | 2.34 | 1.09 | Long Beach |
| 48 | 419148.61 | 5137782.49 | 275.31 | -0.89 | 4.42 | 2.91 | 3.24 | 1.30 | 1.87 | 0.95 | 1.40 | Long Beach |
| 49 | 419189.33 | 5138780.06 | 268.81 | -7.20 | 4.42 | 4.56 | 3.24 | -0.42 | 1.87 | -0.54 | 3.64 | Long Beach |

| Transect ID | StartX (m) | StartY (m) | Azimuth (Degrees) | EPR 1989 to 1999 | ECI 1989 to 1999 | EPR 1999 to 2012 | ECI 1999 to 2012 | EPR 1989 to 2012 | ECI 1989 to 2012 | LRR 1989 to 2012 | LCI95 1989 to 2012 | Region |
|---|---|---|---|---|---|---|---|---|---|---|---|---|
| 50 | 419168.57 | 5139779.85 | 268.81 | -1.81 | 4.42 | 0.97 | 3.24 | -0.21 | 1.87 | 0.34 | 2.17 | Long Beach |
| 51 | 419147.82 | 5140779.63 | 268.81 | -1.58 | 4.42 | 1.59 | 3.24 | 0.25 | 1.87 | 0.57 | 1.80 | Long Beach |
| 52 | 419127.06 | 5141779.42 | 268.81 | -2.91 | 4.42 | 0.02 | 3.24 | -1.22 | 1.87 | -0.22 | 2.60 | Long Beach |
| 53 | 419106.31 | 5142779.20 | 268.81 | -1.51 | 4.42 | 2.28 | 3.24 | 0.68 | 1.87 | 2.50 | 5.69 | Long Beach |
| 54 | 419085.55 | 5143778.99 | 268.81 | -6.38 | 4.42 | 3.92 | 3.24 | -0.44 | 1.87 | -0.10 | 3.25 | Long Beach |
| 55 | 419064.80 | 5144778.77 | 268.81 | -3.44 | 4.42 | 1.88 | 3.24 | -0.37 | 1.87 | 0.74 | 3.69 | Long Beach |
| 56 | 419044.04 | 5145778.55 | 268.81 | 2.65 | 4.42 | 0.13 | 3.24 | 1.20 | 1.87 | 1.90 | 2.69 | Long Beach |
| 57 | 419023.28 | 5146778.34 | 268.81 | -4.10 | 4.42 | 3.15 | 3.24 | 0.08 | 1.87 | -0.15 | 3.66 | Long Beach |
| 58 | 419002.53 | 5147778.12 | 268.81 | -5.70 | 4.42 | 1.87 | 3.24 | -1.34 | 1.87 | -0.29 | 4.14 | Long Beach |
| 59 | 418981.77 | 5148777.91 | 268.81 | -8.07 | 4.42 | 4.73 | 3.24 | -0.69 | 1.87 | 1.51 | 6.55 | Long Beach |
| 60 | 418960.14 | 5149777.67 | 268.70 | -4.28 | 4.42 | 0.15 | 3.24 | -1.72 | 1.87 | 0.07 | 4.56 | Long Beach |
| 61 | 418937.48 | 5150777.42 | 268.70 | -2.74 | 4.42 | 3.99 | 3.24 | 1.14 | 1.87 | 1.60 | 2.50 | Long Beach |
| 62 | 418914.83 | 5151777.16 | 268.70 | -3.06 | 4.42 | 2.27 | 3.24 | 0.01 | 1.87 | 0.10 | 2.69 | Long Beach |
| 63 | 418892.17 | 5152776.90 | 268.70 | -4.31 | 4.42 | 1.40 | 3.24 | -1.01 | 1.87 | -0.56 | 2.68 | Long Beach |
| 64 | 418869.52 | 5153776.65 | 268.70 | -4.53 | 4.42 | 2.47 | 3.24 | -0.49 | 1.87 | 0.80 | 2.86 | Long Beach |
| 65 | 418846.86 | 5154776.39 | 268.70 | -4.61 | 4.42 | 3.76 | 3.24 | 0.22 | 1.87 | 0.42 | 3.54 | Long Beach |
| 66 | 418824.21 | 5155776.13 | 268.70 | -6.09 | 4.42 | 4.46 | 3.24 | -0.01 | 1.87 | 0.62 | 3.49 | Long Beach |
| 67 | 418786.45 | 5156775.29 | 266.87 | -5.48 | 4.42 | 4.04 | 3.24 | 0.01 | 1.87 | 0.42 | 3.59 | Long Beach |
| 68 | 418731.83 | 5157773.80 | 266.87 | -5.52 | 4.42 | 4.58 | 3.24 | 0.31 | 1.87 | 0.97 | 3.98 | Long Beach |
| 69 | 418677.22 | 5158772.31 | 266.87 | 1.34 | 4.42 | 1.29 | 3.24 | 1.31 | 1.87 | 1.40 | 3.55 | Long Beach |
| 70 | 418622.61 | 5159770.82 | 266.87 | -2.84 | 4.42 | 4.57 | 3.24 | 1.43 | 1.87 | 1.46 | 4.76 | Long Beach |
| 71 | 418567.99 | 5160769.32 | 266.87 | -1.93 | 4.42 | 3.74 | 3.24 | 1.34 | 1.87 | 2.03 | 3.67 | Long Beach |

| Transect ID | StartX (m) | StartY (m) | Azimuth (Degrees) | EPR 1989 to 1999 | ECI 1989 to 1999 | EPR 1999 to 2012 | ECI 1999 to 2012 | EPR 1989 to 2012 | ECI 1989 to 2012 | LRR 1989 to 2012 | LCI95 1989 to 2012 | Region |
|---|---|---|---|---|---|---|---|---|---|---|---|---|
| 72 | 418513.38 | 5161767.83 | 266.87 | 3.10 | 4.42 | 1.78 | 3.24 | 2.34 | 1.87 | 2.34 | 3.55 | Long Beach |
| 73 | 418458.76 | 5162766.34 | 266.87 | 1.74 | 4.42 | 3.22 | 3.24 | 2.59 | 1.87 | 3.18 | 4.47 | Long Beach |
| 74 | 418404.15 | 5163764.85 | 266.87 | -3.89 | 4.42 | 9.21 | 3.24 | 3.67 | 1.87 | 4.36 | 6.70 | Long Beach |
| 75 | 418360.09 | 5164763.81 | 268.18 | -6.79 | 4.42 | 10.65 | 3.24 | 3.27 | 1.87 | 3.54 | 6.12 | Long Beach |
| 76 | 418586.14 | 5165694.10 | 301.88 | -5.72 | 4.42 | 13.50 | 3.24 | 5.36 | 1.87 | 6.01 | 6.00 | Long Beach |
| 77 | 419175.03 | 5166495.03 | 315.01 | 25.35 | 4.42 | 18.49 | 3.24 | 21.39 | 1.87 | 20.91 | 5.05 | Long Beach |
| 78 | 425284.83 | 5173029.62 | 202.33 | -0.51 | 4.42 | -2.11 | 3.24 | -1.43 | 1.87 | -1.12 | 2.65 | North Cove |
| 79 | 424359.83 | 5173409.59 | 202.33 | 26.16 | 4.42 | 13.47 | 3.24 | 18.84 | 1.87 | 25.31 | 24.67 | North Cove |
| 80 | 423508.09 | 5173895.64 | 226.93 | -33.33 | 4.42 | -25.69 | 3.24 | -28.92 | 1.87 | -15.18 | 43.56 | North Cove |
| 81 | 422825.21 | 5174626.17 | 226.93 | -25.35 | 4.42 | -6.43 | 3.24 | -85.57 | 1.87 | -18.02 | 8.99 | North Cove |
| 82 | 422142.33 | 5175356.69 | 223.95 | -4.05 | 4.42 | -9.96 | 3.24 | -95.24 | 1.87 | -8.69 | 2.96 | North Cove |
| 83 | 421245.23 | 5175752.40 | 198.29 | -20.88 | 4.42 | -43.30 | 3.24 | -124.96 | 1.87 | -25.89 | 34.17 | North Cove |
| 84 | 420295.75 | 5176066.25 | 198.29 | -3.62 | 4.42 | -28.54 | 3.24 | -126.61 | 1.87 | -10.59 | 15.46 | North Cove |
| 85 | 419346.28 | 5176380.10 | 198.29 | -1.84 | 4.42 | -1.80 | 3.24 | -1.81 | 1.87 | 0.43 | 7.58 | North Cove |
| 86 | 418396.81 | 5176693.94 | 198.29 | -20.04 | 4.42 | -3.13 | 3.24 | -10.29 | 1.87 | -10.17 | 5.62 | North Cove |
| 87 | 417623.70 | 5177287.92 | 226.10 | -67.26 | 4.42 | -17.19 | 3.24 | -38.38 | 1.87 | -29.55 | 20.53 | North Cove |
| 88 | 416930.26 | 5178008.43 | 226.10 | -36.82 | 4.42 | -13.40 | 3.24 | -23.31 | 1.87 | -28.11 | 14.50 | North Cove |
| 89 | 416744.53 | 5178907.01 | 275.25 | 25.67 | 4.42 | 9.10 | 3.24 | 16.11 | 1.87 | 19.73 | 15.41 | North Cove |
| 90 | 416836.04 | 5179902.81 | 275.25 | 0.21 | 4.42 | 50.96 | 3.24 | 29.48 | 1.87 | 33.27 | 17.07 | North Cove |
| 91 | 416812.60 | 5180898.83 | 264.96 | -3.17 | 4.42 | 36.97 | 3.24 | 19.98 | 1.87 | 23.36 | 12.66 | North Cove |
| 92 | 416724.72 | 5181894.96 | 264.96 | -2.99 | 4.42 | 20.76 | 3.24 | 10.71 | 1.87 | 10.46 | 8.24 | North Cove |
| 93 | 416636.85 | 5182891.09 | 264.96 | -5.05 | 4.42 | 12.82 | 3.24 | 5.26 | 1.87 | 4.92 | 10.19 | North Cove |

| Transect ID | StartX (m) | StartY (m) | Azimuth (Degrees) | EPR 1989 to 1999 | ECI 1989 to 1999 | EPR 1999 to 2012 | ECI 1999 to 2012 | EPR 1989 to 2012 | ECI 1989 to 2012 | LRR 1989 to 2012 | LCI95 1989 to 2012 | Region |
|---|---|---|---|---|---|---|---|---|---|---|---|---|
| 94 | 416548.97 | 5183887.22 | 264.96 | -9.91 | 4.42 | 7.27 | 3.24 | 0.00 | 1.87 | 1.32 | 9.42 | North Cove |
| 95 | 416461.10 | 5184883.35 | 264.96 | -12.48 | 4.42 | 7.22 | 3.24 | -1.12 | 1.87 | 0.94 | 9.77 | North Cove |
| 96 | 416323.18 | 5185873.05 | 260.40 | -9.75 | 4.42 | 4.95 | 3.24 | -1.27 | 1.87 | -0.08 | 7.36 | North Cove |
| 97 | 416156.38 | 5186859.04 | 260.40 | -9.29 | 4.42 | 2.44 | 3.24 | -2.53 | 1.87 | -1.82 | 4.57 | North Cove |
| 98 | 415989.58 | 5187845.04 | 260.40 | -7.82 | 4.42 | 2.60 | 3.24 | -1.81 | 1.87 | -0.83 | 3.78 | North Cove |
| 99 | 415822.78 | 5188831.03 | 260.40 | 0.88 | 4.42 | -2.89 | 3.24 | -1.29 | 1.87 | -1.15 | 2.07 | North Cove |
| 100 | 415655.98 | 5189817.02 | 260.40 | -1.39 | 4.42 | -3.70 | 3.24 | -2.72 | 1.87 | -3.41 | 2.05 | North Cove |
| 101 | 415489.19 | 5190803.01 | 260.40 | -1.56 | 4.42 | -3.78 | 3.24 | -2.84 | 1.87 | -4.11 | 2.68 | North Cove |
| 102 | 415322.39 | 5191789.00 | 260.40 | -6.07 | 4.42 | -5.02 | 3.24 | -5.46 | 1.87 | -5.69 | 0.54 | North Cove |